

Preparation and anti-corrosion Properties of SiO₂@MWCNTs@PFOTES Superhydrophobic Coatings on Magnesium Alloy

Zhiqiang Qian^{1,2,*}, Zhong Liu^{1,2}, Shidong Wang^{1,2}, XiuShen Ye^{1,2}, Zhijian Wu^{1,2}

¹ Key Laboratory of Comprehensive and Highly Efficient Utilization of Salt Lake Resources, Qinghai Institute of Salt Lakes, Chinese Academy of Sciences, Xining, Qinghai 810008, China

² Qinghai Provincial Key Laboratory of Resources and Chemistry of Salt Lake, Xining, Qinghai 810008, China

*E-mail: qianzq@isl.ac.cn; zjwu@isl.ac.cn

Received: 28 September 2021 / Accepted: 7 November 2021 / Published: 6 December 2021

Inspiration from nature provides the combination of micro-nano particles and low surface energy materials, a spraying method has been employed to prepare SiO₂@MWCNTs@PFOTES superhydrophobic coatings on magnesium alloy, which can enhance corrosion resistance and coating stability. The prepared coating is composed of silicon dioxide (SiO₂) particles obtained by hydrolysis and condensation reaction of ethyl orthosilicate (TEOS), and carboxylate modified carbon nanotubes (MWCNTs) as rough structure, and 1H, 1H, 2H, 2H-Perfluorooctyltriethoxysilane (PFOTES) as the fluorine silane coupling agent. The coating's composition is determined using field emission scanning electron microscopy (FESEM) and Fourier transform infrared (FTIR) spectroscopy. The polarization curve and electrochemical impedance spectroscopy (EIS) are used to investigate the corrosion resistance of the prepared superhydrophobic surface. Through the salt spray test, the salt resistance of the coating is further discussed. The corrosion current density after the coating is more than four orders of magnitude lower than that of bare magnesium alloy AZ31B, and the water contact angle increases from ~32° to more than 162°. The mechanical, chemical and environmental stability of the superhydrophobic coating has been proved through wear test, immersion test and salt spray test.

Keywords: Superhydrophobic coating; Mg alloy; Corrosion resistance; Salt spray

1. INTRODUCTION

Because of their low density, high specific strength and specific rigidity, excellent electromagnetic shielding performance, low processing cost, easy forming, etc., magnesium (Mg) alloy has received tremendous attention from both engineers and researchers, and has been widely used in the automotive industry, optical equipment, electronics industry, aerospace, and other fields. However, Mg

is more active than the other engineering materials, making Mg alloys have a poor corrosion resistance, which limited their larger scale applications, especially in special environments (such as seawater, organic/inorganic salt solutions, etc.) [1]. As a result, reducing direct contact between magnesium alloy substrates and the erosion medium is critical to reducing corrosion of magnesium alloys and expanding their application. Building an anti-corrosion coating on the surface of a magnesium alloy is one of the most extensive and effective ways to improve corrosion resistance based on this consideration [2-3]. Anti-corrosion coatings are currently being developed using a variety of techniques, including chemical conversion, anodic oxidation, micro-arc oxidation, vapor deposition, electrodeposition, superhydrophobic coatings, etc. [4-8]. Among all the strategies, the superhydrophobic coating is considered an efficient and promising method, due to the micro/nanostructure of superhydrophobic coating can trap a stable air cushion layer on the solid-liquid surface, which can isolate the corrosive medium and the anti-corrosion coatings, and thereby significantly enhancing the corrosion resistance of Mg alloys and extending the service life of the coatings [9].

Numerous techniques have been developed and applied to avoid direct contact between the substrate and the corrosive medium since the development of superhydrophobic technology in the corrosion protection of magnesium and magnesium alloys, including the hydrothermal process, chemical deposition, electrodeposition techniques, conversion coatings, polymer coatings, etching, sol-gel coatings, etc [10-15]. In general, constructing a hierarchical structure on the surface of magnesium alloys and modifying the rough film with a low surface energy substance are two indispensable and imperative processes for preparing superhydrophobic surfaces on the surface of magnesium alloys. However, most of these preparation methods have many shortcomings, such as multi-step process, tedious chemical treatments, time-consuming, etc., which restrict their large-scale and practical application [16]. Both surface roughness and low surface energy should be obtained in one step to overcome these disadvantages and simplify the complexity of multi-step processing. Therefore, developing and preparing superhydrophobic surfaces on magnesium alloys with a simple and feasible one-step method is considered worthwhile. In the recent works, a simple spray technique is employed to manufacture superhydrophobic surface, which not only has excellent performance such as simple operation, low cost and short time-consuming, but also can be easy to re-heal any damages by just re-spraying the coating solution when the superhydrophobic surfaces are damaged or degenerated. [17]

Carbon nanotubes (CNTs) could produce multi-scale microstructures and thus surface roughness due to their unique nanostructure, intrinsic hydrophobic graphitic surface, and higher length-to-diameter ratio, making them nanomaterials for rough superhydrophobic coatings with improved mechanical properties [18-20]. Although the superhydrophobic CNFs film displayed an excellent water-repellent property (WCA > 167°, WCA hysteresis < 5°), the modification process was relatively complicated, and not feasible on a large scale [21]. In comparison to adding only CNTs, a small amount of hydrophobic SiO₂ nanoparticles can further improve the surface roughness of the coatings, resulting in improved self-cleaning properties. Furthermore, combining CNTs with TiO₂ nanoparticles would exhibit a synergistic effect to fabricate superhydrophobic coatings with better mechanical strength and durability [22]. There is no link between CNT incorporation and waterborne coating corrosion performance. In this study, MWCNTs/SiO₂ composites superhydrophobic films were prepared by spraying on the AZ31B

Mg alloy. Electrochemical, long-term static, seawater immersion (3.5 wt percent NaCl solution), and salt spray corrosion were used to assess corrosion behavior and mechanism, respectively.

2. EXPERIMENTAL

2.1 Materials and reagents

The AZ31B Mg alloy (composition: Al 2.98 wt%, Zn 0.84 wt %, Mn 0.34wt%, Si 0.01 wt%, with the balance being Mg) was purchased from Dongguan Hongxing Metal Materials Co., Ltd. The dimension of the AZ31B plates was 60 mm × 40 mm × 3 mm. Shanghai Aladdin Biochemical Technology Co., Ltd provided 5 wt% Multi-wall carbon nanotubes MWCNTs dispersion aqueous solution. Tetraethoxysilane (TEOS, 98%) was bought from Sinopharm Chemical Reagent Co., Ltd. 1H,1H,2H,2H-perfluorooctyltriethoxysilane (PFOTES, 97%) with a chemical formula of $\text{CF}_3(\text{CF}_2)_5(\text{CH}_2)_2\text{-Si}(\text{OCH}_2\text{CH}_3)_3$ was purchased from Shanghai Adamas Chemical Reagent Co., Ltd. All the other reagents, including ethanol, strong ammonia (25% NH_3), Na_2CO_3 , Na_2SO_4 , NaOH, NaCl, were analytically pure and were obtained from Sinopharm Chemical Reagent Co. Ltd.

2.2 Preparation of the superhydrophobic surfaces

(1) Pretreatment of magnesium alloys

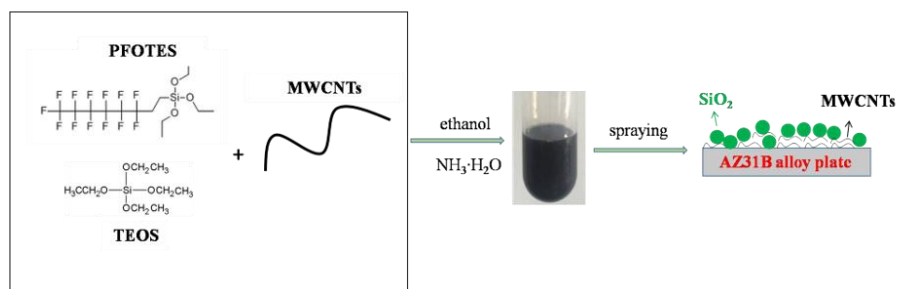
All of the plate samples were sequentially polished with 320, 800, and 2000 grit silicon carbide water abrasive papers prior to the construction of a superhydrophobic film on the AZ31B Mg alloy surface. After that, the plate sample was ultrasonically cleaned three times in ethanol and water, followed by air drying.

(2) Preparation of suspensions

First, add a certain amount of carbon nanotubes (MWCNTs) aqueous solution to 20 mL of ethanol, and ultrasonically disperse for 30 minutes; then add a certain amount of concentrated ammonia to the beaker, and magnetically stir for 30 minutes at room temperature to mix evenly. Finally, to prepare the spray solution, TEOS and PFOTES were slowly added to the beaker and stirred for 12 hours.

(3) Preparation of superhydrophobic coating

Superhydrophobic coatings are made using the spraying method. A spray gun (Infinity, Harder & Steenbeck, Germany) was used to spray 4 mL of a mixture containing MWCNT and silica particles onto the surface of the AZ31B alloy at a pressure of 0.2 MPa N_2 . The spray gun's tip is 15 cm away from the surface of the AZ31B alloy during the spraying process. To speed up solvent evaporation, a hot plate is used to heat the AZ31B alloy sample pretreated during spraying. The samples were then heated for 1 h at 100°C after coating. In comparison, spraying was used to create coatings containing only MWCNTs or SiO_2 . The preparation process is shown in Schematic 1.



Schematic 1 Schematic illustration of preparation of superhydrophobic surface coatings.

2.3 Characterization

The morphologies and structures of the prepared materials were observed using field emission scanning electron microscopy (FESEM, Hitachi SU8010) and Fourier transform infrared (FTIR, Thermo Nicolet). DSA25 optical contact angle measuring instrument (Kruss, Germany) was used to measure the static contact angle and sliding angle of different solution droplets with a volume of $5\mu\text{L}$ on the superhydrophobic surface at room temperature according to the static drop method. In about 5 sec, the contact angle value is determined. All measurements were repeated five times, with the average value being used for discussion.

2.4 Electrochemical tests

All electrochemical measurements were performed using a CHI604E electrochemical workstation (Shanghai Chenghua Instrument Co., Ltd, China). A three-electrode device was used, with a platinum plate serving as an auxiliary electrode, a saturated calomel electrode serving as a reference electrode, and the test sample serving as a test electrode. The tested sample's exposure area was 1 cm^2 .

At a scan rate of 1 mV s^{-1} , the polarization curves were obtained in a 3.5 wt% NaCl solution. The corrosion current density (I_{corr}), corrosion potential (E_{corr}), and Tafel constant were determined using the extrapolation method. The polarization tests were repeated five times to confirm the dependability of the electrochemical parameters, and the average values were obtained. The protection efficiency (η) is calculated by the formula (1) [23]:

$$\eta = (i_{\text{cor}}^0 - i_{\text{cor}}) / i_{\text{cor}}^0 \times 100\% \quad (1)$$

Among them, η is the protection efficiency of the coating, and i_0 and i respectively represent the corrosion current density values of the substrate and the coating.

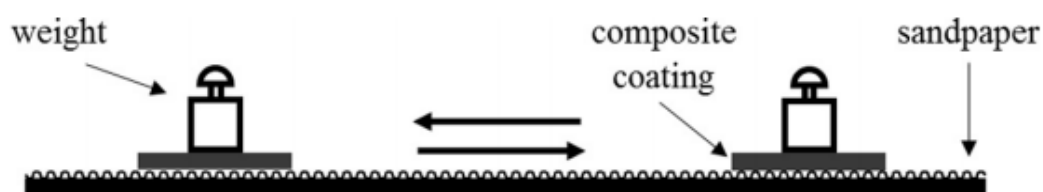
Electrochemical impedance spectroscopy (EIS) was obtained at room temperature from 100 kHz to 10 mHz using a $5\text{ mV} \cdot \text{s}^{-1}$. Before the electrochemical test, the sample was immersed in a 3.5 wt% NaCl solution for 30 minutes.

2.5 Adhesion and abrasion resistance test

The coating adhesion cross-cut method test standard (ASTM D 3359) is used to assess the

adhesion between the superhydrophobic film and the magnesium alloy substrate [24]. The experiment was carried out with Elcometer 107, which was used to make 6 parallel cuts with equal spacing (1mm) on the coating, and then cut perpendicularly the cuts with the same number and spacing as the former, and the adhesion was evaluated by the peeling area of the coating surface.

The superhydrophobic coating's abrasion resistance was tested using sandpaper. Schematic 2 illustrates the test device. A 50-gram weight and 1200-grit sandpaper make up the majority of the test device. The superhydrophobic film is first placed in contact with the sandpaper, then the weight is placed on the magnesium alloy that has been prepared. The sample is then rotated 90° (the side of the film facing the sandpaper) and moved another 10 cm in the opposite direction after the superhydrophobic film has been pushed 10 cm in the opposite direction. A wear cycle is a term for the entire process described above. Following the abrasion test, the superhydrophobic film's contact angle and rolling angle were measured.



Schematic 2. The schematic of friction test (50-gram weight, 1200-grit sandpaper, one wear cycle is 20 cm)

2.6 Corrosion tests

The samples were tested by immersing them in 3.5 wt.% NaCl solution, immersing in different pH solutions, exposing to air, and salt spray tests to investigate their corrosion resistance and stability in aqueous medium and atmospheric conditions.

For the corrosion test in atmospheric conditions, the samples were placed into a salt spray test chamber (LYW-015, Shanghai Lanbao Testing Equipment Manufacturing Co., Ltd., China.), and the salt spray test is tested following ASTM B117. The sample was placed at a 30° angle with the plane of the corrosion box during the experiment, and the solution in the experiment box was fully atomized to simulate the slow deposition of salts on the surface of the sample in the actual environment. The salt spray chamber temperature is 35°C, the pressure barrel temperature is 47°C, and the 5 wt.% NaCl solution has a pH value of 6.5-7.2. According to the requirements of the equipment, the inlet pressure is 0.35 MPa, the spray pressure is 0.05 MPa, and the salt spray precipitation is 1-2 mL/h. Every 24 hours during the salt spray corrosion test, samples were taken out of the salt spray corrosion chamber to observe surface corrosion and test the wettability of the surface.

3. RESULTS AND DISCUSSION

3.1 Surface morphology and composition

FESEM was used to characterize the coating morphologies, and the test results are shown in Figure 1. The contact angle and corrosion current density under various compositions were investigated in order to find the best solution composition (Figure S1–Figure S4). Under the optimal conditions, the contact angle of the composite film layer is 161.8° , and the rolling angle is 1.6° . As shown in Fig.1(a), TEOS hydrolysis produces SiO_2 microspheres with a diameter of about $0.5\text{--}1\ \mu\text{m}$ that covers the magnesium alloy's surface. A superhydrophobic coating is formed on the magnesium alloy after the surface energy is reduced by PFOTES. Figure 1(b) illustrates that MWCNTs are randomly stacked on the surface of the magnesium alloy to form a large number of holes. The pore structure can trap air and PFOTES is similar to an adhesive to connect MWCNTs, which would be increased the hydrophobicity of the surface (the contact angle of the coating is 135°) [24]. Figure 1 (c, d) shows the morphology of $\text{SiO}_2/\text{MWCNTs}/\text{PFOTES}$ at the optimal ratio. It can be found that the SiO_2 microspheres formed by hydrolysis in the composite coating are distributed on the entire magnesium alloy surface, while the MWCNTs agglomerate and intersect in the gaps between the SiO_2 microspheres, thus increasing the coating's density and stability [25]. MWCNTs are randomly stacked in the middle of SiO_2 microspheres to form a large number of pore structures, as shown in Figure 1(d), and the MWCNTs are firmly attached to the SiO_2 surface.

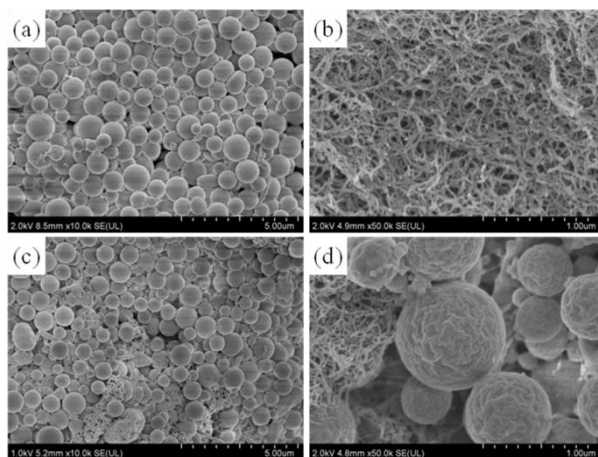


Figure1. The surface topography of the coatings (a: $\text{SiO}_2/\text{PFOTES}$, b: $\text{MWCNTs}/\text{PFOTES}$, c and d: $\text{SiO}_2/\text{MWCNTs}/\text{PFOTES}$)

Based on the optimal solution ratio, the chemical composition of the composite coating was analyzed by FT-IR. Fig.2 shows the infrared test results of $\text{SiO}_2/\text{PFOTES}$, $\text{MWCNTs}/\text{PFOTES}$ and $\text{SiO}_2/\text{MWCNTs}/\text{PFOTES}$ composite coatings. Figure 2 shows that the peak at $3420\ \text{cm}^{-1}$ is attributed to the stretching vibration peak of the OH bond, and $2942\ \text{cm}^{-1}$ and $2863\ \text{cm}^{-1}$ are attributed to the $-\text{CH}_2\text{CH}_3$ absorption peak in PFOTES, $481\ \text{cm}^{-1}$, $801\ \text{cm}^{-1}$ and $1108\ \text{cm}^{-1}$ are attributed to the Si-O-Si symmetric

stretching vibration, bending vibration, and rocking vibration generated during TEOS hydrolysis, respectively. The composition form of the CF bond in PFOTES in the SiO₂/PFOTES coating is attributed to the peaks at 595 cm⁻¹ and 1219 cm⁻¹, proving that the SiO₂/PFOTES coating is composed of Si-O-Si modified by PFOTES [26-28]. The stretching vibration peak of the OH bond is attributed to 3432 cm⁻¹, the -CH₂CH₃ absorption peaks in PFOTES are attributed to 2912 cm⁻¹ and 2839 cm⁻¹, and the silsesquioxane band is attributed to 1162 cm⁻¹ and 1270 cm⁻¹ during the hydrolysis and condensation process of PFOTES, and the characteristic peak of -COOH at 1446 cm⁻¹ belongs to the C-O stretching vibration peak of acidified carbon nanotubes coating MWCNTs/PFOTES [29-30]. In the SiO₂/MWCNTs/PFOTES coating, in addition to the characteristic peaks in SiO₂/PFOTES and MWCNTs/PFOTES, a C=O vibration peak appears at 1386 cm⁻¹, which is due to the esterification reaction between of -COOH of MWCNTs and -OH formed from TEOS hydrolysis [31].

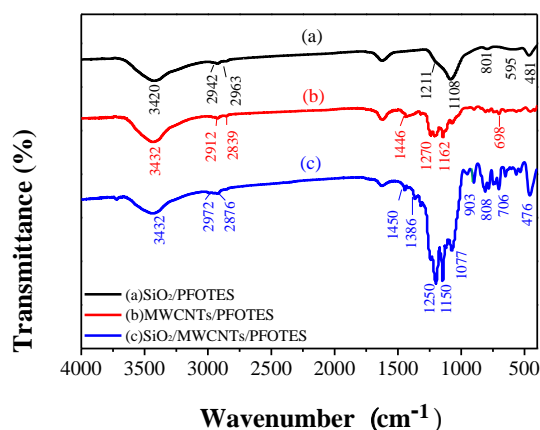


Figure 2. FTIR spectra of (a: SiO₂/PFOTES coatings, b: MWCNTs/PFOTES coatings, c: SiO₂/MWCNTs/PFOTES coatings)

3.2 Corrosion resistance properties

MWCNTs are well known for their potential to act as a physical barrier to corrosive substances attacking a substrate. However, the corrosion resistance of magnesium alloys is not significantly improved by the superhydrophobic coating composed of MWCNTs and silica. The electrochemical polarization curve test can be employed to obtain two important parameters that characterize the corrosion performance (one is the corrosion current density, which reflects the corrosion rate; the other is the corrosion potential, which reflects the trend of the corrosion reaction.), which can be used to indicate the corrosion resistance performance of the superhydrophobic surface [32-35]. The electrochemical polarization curve tests were used to investigate the effect of MWCNT doping in the coating on corrosion resistance, and the results are shown in Figure 3. As can be seen from Fig.3, the corrosion current densities (i_{corr}) of SiO₂/PFOTES, MWCNTs/PFOTES and SiO₂/MWCNTs/PFOTES coatings are 3.869×10^{-8} A/cm², 8.598×10^{-5} A/cm² and 9.474×10^{-9} A/cm² respectively, the corrosion voltage (E_{corr}) is -1.483 V, -1.374 V and -1.370 V, respectively. Compared with the i_{corr} (3.692×10^{-5} A/cm²)

and E_{corr} (-1.577 V) of bare magnesium alloy, indicating that the $\text{SiO}_2/\text{PFOTES}$ and $\text{SiO}_2/\text{MWCNTs}/\text{PFOTES}$ coatings can hinder the corrosion of the magnesium alloy substrate. In addition, the i_{corr} of the $\text{SiO}_2/\text{MWCNTs}/\text{PFOTES}$ coating is reduced by about 4 orders of magnitude, and the E_{corr} is positively shifted by about 0.2 V, suggesting that adding MWCNTs to the $\text{SiO}_2/\text{PFOTES}$ can improve the corrosion resistance, which is attributed to the formation of -Si-O-Si-, -COOSi and other covalent bonds in the $\text{SiO}_2/\text{MWCNTs}/\text{PFOTES}$ coating, and also due to the increased compactness of the coating with MWCNTs, thereby effectively preventing the penetration of corrosive media ions and inhibiting the diffusion of corrosion products [36]. In addition, a passivation zone exists in the anode area of the $\text{SiO}_2/\text{MWCNTs}/\text{PFOTES}$ coating's polarization curve. This is because MWCNTs and SiO_2 particles form a dense coating on the surface of the substrate to limit the occurrence of anodic reactions, thereby inhibiting the progress of corrosion and improving the corrosion resistance [37].

The polarization parameters were fitted to quantify the corrosion resistance of the composite coating. As shown in Table 1, the protection efficiency of $\text{SiO}_2/\text{MWCNTs}/\text{PFOTES}$ coating reached 99.97%. In addition, the parameters β_a and β_c in Table 1 represent the slope of the anodic polarization curve and the slope of the cathodic polarization curve, respectively. Polarization resistance (R_p) is related to β_a , β_c and i_{corr} and is calculated according to formula (1). The corrosion resistance of the $\text{SiO}_2/\text{MWCNTs}/\text{PFOTES}$ superhydrophobic coating is 4 orders of magnitude higher than the bare AZ31B magnesium alloy, indicating that the superhydrophobic surface has an excellent anti-corrosion effect, according to the corrosion resistance R_p parameter.

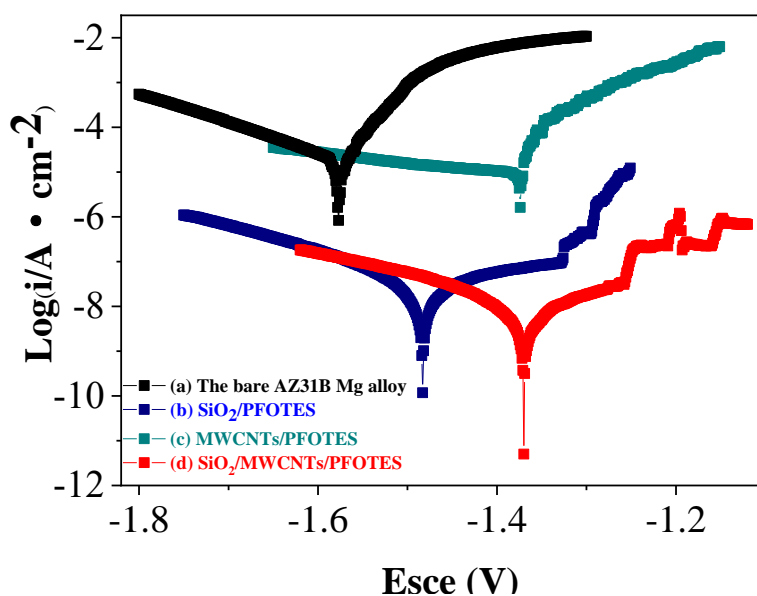


Figure 3. Tafel polarization curves in 3.5wt.% NaCl solution at room temperature: a: bare AZ31B Mg alloy, b: $\text{SiO}_2/\text{PFOTES}$ coatings, c: MWCNTs/PFOTES coatings, d: $\text{SiO}_2/\text{MWCNTs}/\text{PFOTES}$ coatings. The scanning rate was 1 mV/s.

Table 1. Corrosion parameters obtained from polarization curve of the samples

Sample	Corrosion potential	Corrosion current density	Tafel constant		Corrosion impedance	Protection efficiency
	E_{corr} (V)	i_{corr} ($\text{A}\cdot\text{cm}^{-2}$)	β_a (V/dec)	β_c (V/dec)	R_p (Ω)	η (%)
bare AZ31B	-1.577	3.692×10^{-5}	0.147	0.065	5.3×10^2	-
SiO ₂ /PFOTES	-1.483	3.869×10^{-8}	0.273	0.138	1.0×10^6	98.9
MWCNTs/PFOTES	-1.374	8.598×10^{-5}	0.097	0.586	4.2×10^2	-
SiO ₂ /MWCNTs/PFOTES	-1.370	9.474×10^{-9}	0.109	0.151	2.9×10^6	99.7

As shown in Figure 4, the EIS spectra of the bare AZ31B, the SiO₂/PFOTES coatings, the MWCNTs/PFOTES coatings, the SiO₂/MWCNTs/PFOTES coatings are obtained after immersion in 3.5 wt. % NaCl aqueous solution, respectively. Generally, EIS testing is considered to be an effective method to analyze the corrosion characteristics of metal coatings [38]. The results of the Nyquist plot show a completely different capacitance loop, which can be attributed to the charge transfer resistance of the corrosion process, while the Nyquist plot of the SiO₂/MWCNTs/PFOTES coatings included larger diameter capacitive loops. The diameter of the capacitor circuit is usually proportional to the corrosion rate, that is, the larger the diameter, the smaller the corrosion rate [39], which corresponds to the polarization curves.

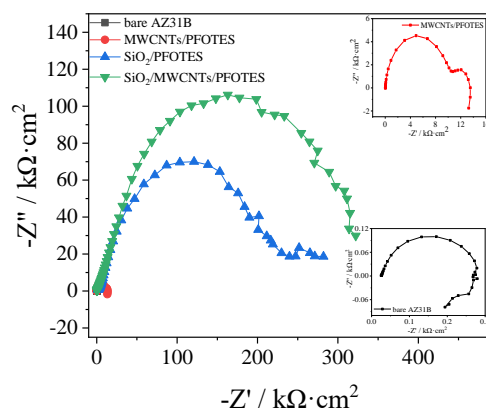


Figure 4. The Nyquist plots obtained from the bare AZ31B Mg alloy, the SiO₂/PFOTES coatings, the MWCNTs/PFOTES coatings, the SiO₂/MWCNTs/PFOTES coatings after immersion in 3.5 wt. % NaCl aqueous solution for 30 min.

3.3 Stability properties of superhydrophobic coating

The chemical stability of the superhydrophobic surface is a key factor that determines its feasibility in industrial applications. As a result, using an acid-base solution and air exposure method, the chemical stability of the obtained superhydrophobic surface was investigated.

Figure 5 shows the contact angle and rolling angle of water droplets of different pH solutions to the superhydrophobic surface. The contact angle is maintained above 154° and the rolling angle is below 10° in the pH range of 1–14, indicating that acidity and alkalinity have little effect on the superhydrophobic properties of the prepared superhydrophobic coating.

To investigate the change of surface wettability of superhydrophobic samples in the air, the prepared samples were exposed to air at a room temperature of $20\text{--}25^\circ$ and a relative humidity of 30%–50%, and the contact angle and roll angle was tested every 10 days, as shown in Figure 6. The contact angle and roll angle was tested every 10 days. Although the contact angle decreased slightly after 2 months in the air, it remained above 150° , indicating that the superhydrophobic surface has good air stability.

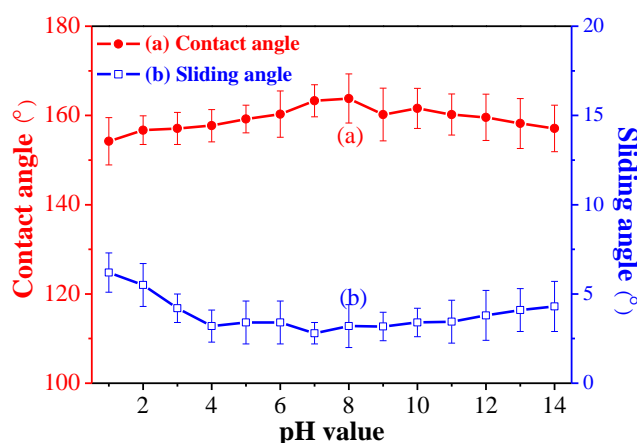


Figure 5. The relationship between the pH value and the CA and the SA of the superhydrophobic surfaces (pH range is 1–14).

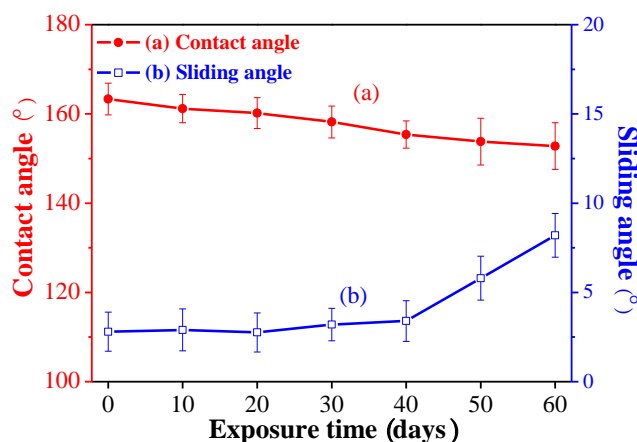


Figure 6. The relationship between the exposure time to air and the CA and the SA of the superhydrophobic surfaces (the prepared samples were exposed to air at a room temperature of $20\text{--}25^\circ$ and a relative humidity of 30%–50%)

Figure 7 shows that after 10 cycles of abrasion test, the contact angle of the coating dropped from 161.2° to 154.8° , and the rolling angle increased from 1.6° to 3.4° , indicating that the composite coating still maintains super-hydrophobicity. The crosshatch tape adhesion test for composite coatings is shown in photos in Figure 8. The lattice does not fall off and the cut edge is smooth after the cross-cut tape adhesion test (Figure 8c). Therefore, the ASTM 5B rating for SiO₂/MWCNTs/PFOTES coating denotes the highest substrate adhesion. However, the other two coatings are rated ASTM 4B and ASTM 2B (Figure 8a and Figure 8b), respectively.

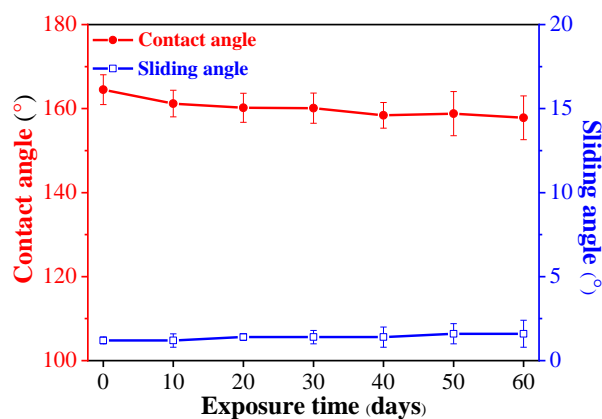


Figure 7. The hydrophobic performance of the superhydrophobic surface after 10 times abrasion testing.

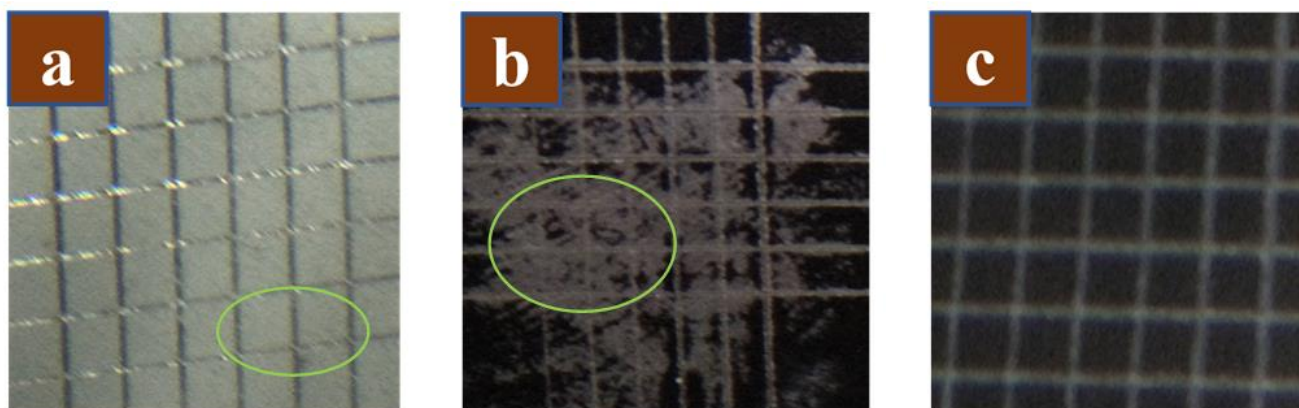


Figure 8. The photos of crosshatch tape adhesion test for the composite coatings: a: SiO₂/PFOTES coatings, b: MWCNTs/PFOTES coatings, c: SiO₂/MWCNTs/PFOTES coatings. (According to ASTM 5B standard)

3.4 Corrosion performance in neutral salt spray test

The majority of metals are found in nature, particularly in direct contact with the moisture, oxygen, sulfur dioxide, and chloride contained in the atmosphere, thereby causing damage or deterioration of the metal materials. Atmospheric corrosion caused by salt spray is very common and

destructive. The salt spray environment is primarily used to evaluate the corrosion resistance of the samples in the simulated salt spray environment.

A continuous neutral salt spray test was performed in a salt spray test box following the ASTM B117 standard. The samples were taken out every 24 h to observe the macroscopic changes on the surface of the samples and photograph them with a digital camera. The surface of the sample after the salt spray experiment is shown in Figure 9. The surface of the bare AZ31B has been completely corroded after a 24 h salt spray test. The depth of surface pitting pits continues to increase as corrosion time increases. However, after the 96 h salt spray test, the SiO₂/MWCNTs/PFOTES coating gradually showed salt spray deposition and pitting corrosion on the surface. The corrosion area on the surface continues to grow as the salt spray time is extended. Although the majority of the surface area retains the film after 168 hours of salt spray corrosion, it can be seen that there are obvious pitting pits and salt deposits on the surface. Although numerous studies have shown that superhydrophobic coatings can improve the corrosion resistance of metals [40], the durability of corrosion resistance during actual use is closely related to the adhesion between the superhydrophobic coating and the substrate [41].

An FESEM was used to characterize the sample at the micro-scale after observing the surface of the sample after the salt spray experiment at the macro level. The results are shown in Figure 10. After salt spray corrosion, the surface of bare AZ31B is composed of flakes that resemble petals, which is due to the contact between the corrosive medium and the magnesium alloy substrate to form a film containing MgO and Mg(OH)₂ [11]. However, as shown in Figure 10(d), the superhydrophobic coating's surface morphology barely changed before and after corrosion, indicating that salt spray corrosion did not affect the structure of the superhydrophobic composite coating.

The contact angle of the sample surface was measured after the salt spray experiment. Due to the composite coating maintains its surface integrity after 144 h of salt spray corrosion, the contact angle is still greater than 150°, as shown in Figure 11, which corresponds to the appearance of the sample in the digital photo of Figure 9.

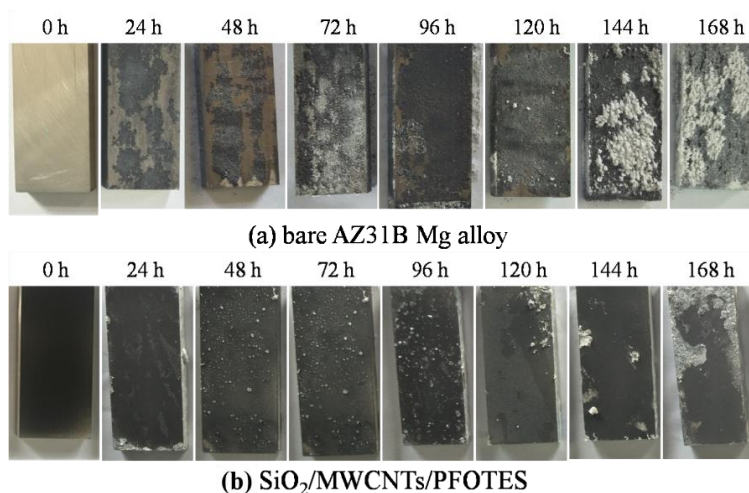


Figure 9. The optical surface photo after salt spray experiment: (a) bare AZ31B Mg alloy, (b) SiO₂/MWCNTs/PFOTES coatings. (The test is carried out in accordance with ASTM B117 standard for continuous neutral salt spray test. The samples were taken out every 24 hours and photographed with a digital camera.)

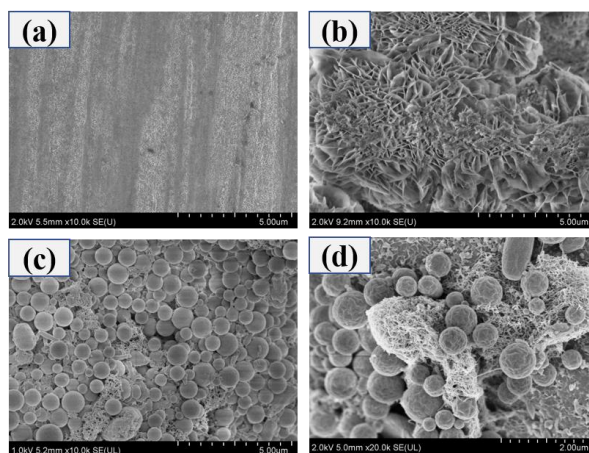


Figure 10. The surface morphology before and after the salt spray experiment (a) bare AZ31B Mg alloy-0h, (b) bare AZ31B Mg alloy-168 h, (c) SiO₂/MWCNTs/PFOTES-0h, (d) SiO₂/MWCNTs/PFOTES-168h.

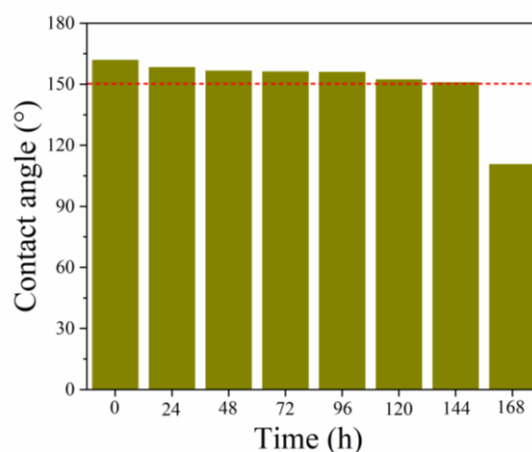


Figure 11. The contact angle after salt spray experiment of SiO₂/MWCNTs/PFOTES coating (the contact angle was tested every 10 days)

4. CONCLUSIONS

A superhydrophobic coating composed of low surface energy materials (PFOTES) and micro-nano rough structures (SiO₂ and MWCNTs) is formed on the surface of AZ31B magnesium alloy. The morphology, chemical composition, and corrosion resistance of various coatings are studied in-depth and in comparison. The main results are summarized as follows:

(1) By adjusting the spraying solution ratio, the optimal solution composition can be obtained. The built SiO₂/MWCNTs/PFOTES magnesium alloy superhydrophobic coating has a contact angle greater than 160° and a rolling angle less than 2° based on the best composition.

(2) The chemical composition and morphology of different coatings were analyzed by FTIR and SEM. The MWCNTs and the hydrolyzed SiO₂ were tightly bonded via covalent bonds in the

SiO₂/MWCNTs/PFOTES coating. Moreover, the addition of MWCNTs improves the SiO₂/MWCNTs/PFOTES coating's compactness and adhesion.

(3) The electrochemical test results show that the corrosion current density of the SiO₂/MWCNTs/PFOTES superhydrophobic composite coating has dropped by 4 orders of magnitude. The prepared superhydrophobic film has a surface contact angle of less than 150° after 10 times of rubbing, and it has superior adhesion to the magnesium alloy substrate, according to the wear and adhesion test results (5B). These results show that the superhydrophobicity coating exhibited good mechanical, chemical, and environmental stability.

(4) The corrosion resistance of the samples was investigated using a neutral salt spray corrosion experiment. The results show that the superhydrophobic surface improves the corrosion resistance better, and the SEM results show that the morphology before corrosion is maintained, which corresponds to the contact angle test results. The hydrophobicity, composition, and microstructure of the superhydrophobic surface are all factors that influence corrosion resistance. However, the application of superhydrophobic coatings in the field of metal corrosion protection needs further in-depth research.

ACKNOWLEDGEMENTS

This work was financially supported by supported by Qinghai Provincial Science and Technology Project, China (2019-ZJ-956), the National Natural Science Foundation of China (U20A20147), Thousand Talent Program of Qinghai Province, China (2019), and the CAS "Light of West China" Program.

SUPPORTING INFORMATION

1 Optimal conditions determination for TEOS and NH₃·H₂O

The hydrolysis of TEOS to obtain SiO₂ of appropriate size plays a vital role in the hydrophobicity and corrosion resistance of the composite film. In this work, the size and content of SiO₂ particles are adjusted by changing the content of NH₃·H₂O and TEOS in the mixed solution. The measurement of the static contact angle and electrochemical polarization were used to investigate the hydrophobic and anti-corrosion properties of the composite film.

Figure S1 and Figure S2 show the effect of NH₃·H₂O and TEOS component variables on the hydrophobicity and corrosion resistance of the composite coatings. It can be seen from Figure S1 that as the content of NH₃·H₂O increases, the contact angle continues to increase and then basically tends to balance, and the contact angle remains at about 156°. When the content of NH₃·H₂O is 0.3 mL, the sliding angle reaches the minimum. The contact angle of the MWCNTs/PFOTES coating (excluding SiO₂) is 138.2°, which shows that although the fluorinated MWCNTs increases the roughness of the composite film, the nano-scale size of MWCNTs is difficult to form a large enough "air cushion" on the surface. Therefore, the contact angle of the coating is less than 150 degrees, that is, no super-hydrophobic surface is formed. When the TEOS content is 0.22 mL, the hydrophobic performance of the composite film achieves the best value, the contact angle of the composite film is 161.8°, and the rolling angle is 1.6°.

To verify the optimal value of each variable in the selection of the condition experiment, the electrochemical polarization curves were used to investigate the electrochemical performance of the composite coating. The results show that the prepared composite coating has the best hydrophobicity and corrosion resistance when the composition of the solution is 0.3 mL and 0.22 mL of $\text{NH}_3 \cdot \text{H}_2\text{O}$ and TEOS, respectively.

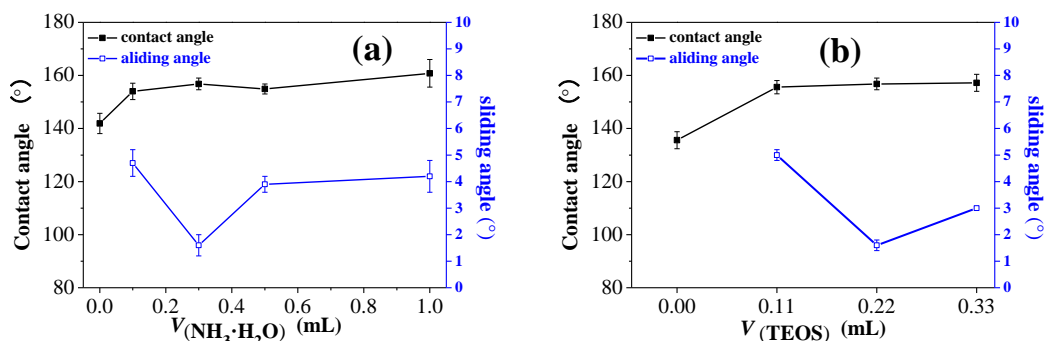


Figure S1 Influence of (a) $\text{NH}_3 \cdot \text{H}_2\text{O}$ and (b) TEOS variable on wettability of the surface ($5\mu\text{L}$ water on the surface at room temperature according to the static drop method)

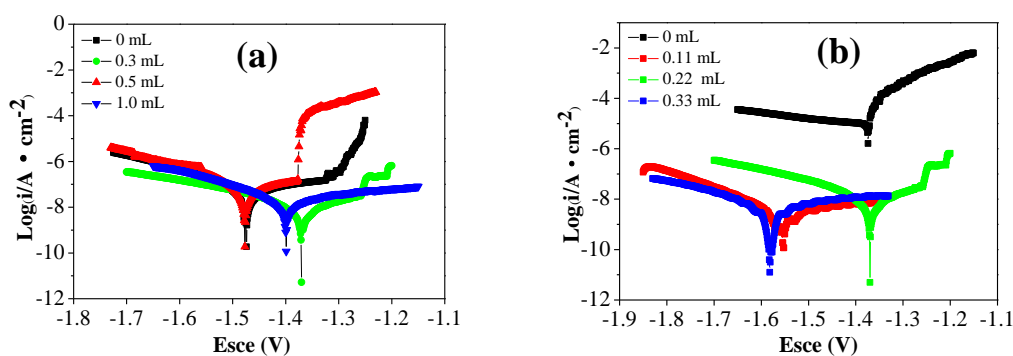


Figure S2. Potentiodynamic polarization curves for each variable in 3.5wt.% NaCl solution at room temperature: a: $\text{NH}_3 \cdot \text{H}_2\text{O}$, b: TEOS. The scanning rate was 1 mV/s.

2 Optimization experiment of MWCNTs and PFOTES

In the $\text{SiO}_2/\text{MWCNTs}/\text{PFOTES}$ composite film, the content of MWCNTs and PFOTES are one of the key factors affecting the performance of the film. Figure S3 and Figure S4 show that the wetting performance and electrochemical performance of the composite coating are affected by MWCNTs and PFOTES as variables, respectively. It can be seen from Figure S3 that the addition of MWCNTs in the mixed solution has little effect on the contact angle and sliding angle. The contact angles are all above 155° within the selected variable range, and the sliding angle is minimized when the MWCNTs solution is added to 1.0 mL. The contact angle $\text{SiO}_2/\text{MWCNTs}$ film is 15.5° , implying that the surface is hydrophilic. With the addition of PFOTES, the surface of the sample changed from hydrophilic to

hydrophobic. When the content of PFOTES increased to 0.52 mL, the contact angle of the sample surface increased to 161.8°, and the rolling angle decreased to 2.2°. Figure S4 shows that the electrochemical performance of the composite coating changes with the content of MWCNTs and PFOTES. The electrochemical results are consistent with the wettability. The results show that superhydrophobic surface can effectively improve the corrosion resistance of the Mg alloy. In addition, it can be inferred that super-hydrophobic performance is consistent with corrosion resistance, in other words, the larger the contact angle and the smaller the rolling angle, the better corrosion resistance.

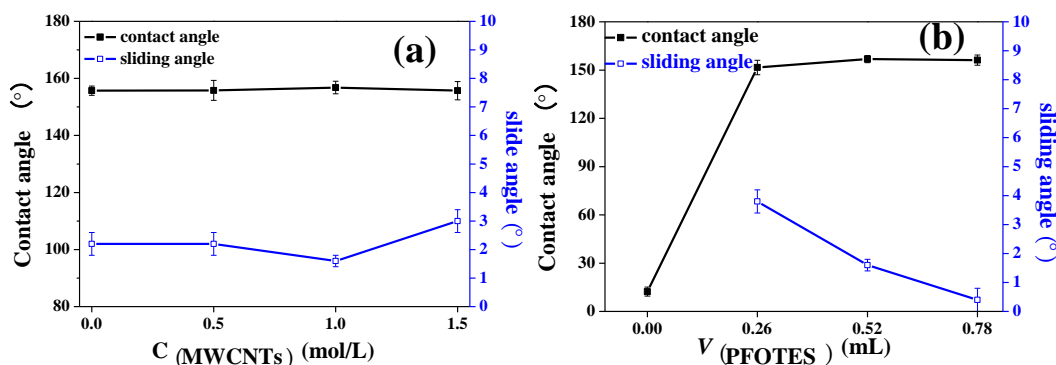


Figure S3 Influence of (a) 5 wt.% MWCNTs solution, (b) PFOTES variable on wettability of the surface (5 μL water on the surface at room temperature according to the static drop method)

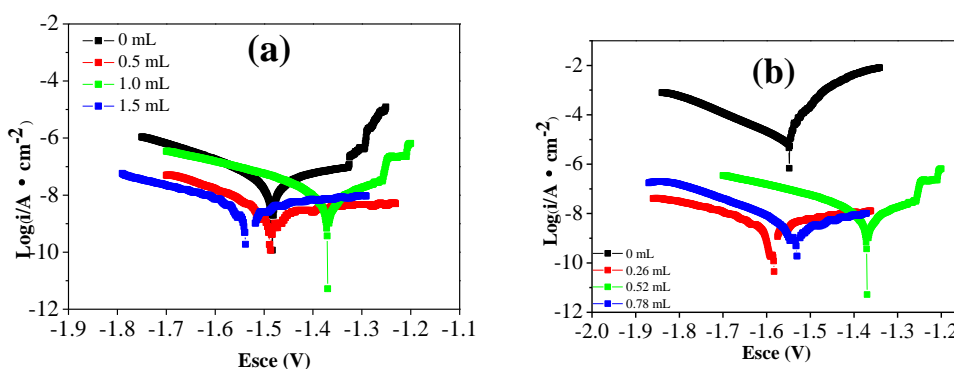


Figure S4. Potentiodynamic polarization curves for each variable in 3.5 wt.% NaCl solution at room temperature: (a) 5 wt.% MWCNTs solution, (b) PFOTES. The scanning rate was 1 mV/s.

Based on the investigation of the influence of different components in the mixed solution on the hydrophobicity, the optimal spraying solution ratio in Table S1 was determined, and the performance of the SiO₂/MWCNTs/PFOTES composite film prepared at the optimal ratio was analyzed.

Table S1 The solution composition

Optimal composition	content (mL)
TEOS	0.22
25% NH ₃ ·H ₂ O	0.30
PFOTES	0.52
5 wt.% MWCNTs aqueous	1.0
Ethanol	20.0

References

1. A.B. Ikhe, A.B. Kale, J. Jeong, M.J. Reece, S.-H. Choi, Pyo M, *Corros. Sci.*, 109 (2016) 238.
2. A. Atrens, G.L. Song, M Liu, A.M. Shi, F.Y. Cao, M. S. Dargusch, *Adv. Eng. Mater.*, 17 (2015) 400.
3. L R Chang, F H Cao, J S Cai, W J Liu, Z Zhang, J. Q. Zhang, *T. Nonferr. Metal. Soc.*, 21 (2011) 307.
4. J. Gray-Munro, J. Campbell, *Mater. Lett.*, 189 (2017) 271.
5. X. Qiu, P. Wan, L. L. Tan, X.M. Fan, K, *Mater. Sci. Eng.*, 36 (2014) 65.
6. S. Sonmez, B. Aksakal, B. Dikicic, *J. Alloy Compd.*, 456 (2014) 125.
7. F. Brusciotti, D.V. Snihirova, H. Xue, M.F. Montemor, S.V. Lamaka, M.G.S. Ferreira, *Corros. Sci.*, 67 (2013) 82.
8. Y. Wu, T Hang, Z Yu, L Xu, M Li, *Chem. Commun.*, 50 (2014) 8405.
9. J.F. Wei, B.C. Li, L.Y. Jing, N. Tian, X. Zhao, J.P. Zhang, *Chem. Eng. J.*, 390 (2020) 124562.
10. N. Yang, J. C. Li, N. N. Bai, L. Xu, Q. Li, *Mater. Sci. Eng. B.*, 209 (2016) 1.
11. L. Wang, J. Y. Yang, Y. Zhu, Z. H. Li, T. Shen, D. Q. Yang, *Mater. Lett.*, 171 (2016) 297.
12. H. R. Wan, X. F. Hu, *Mater. Lett.*, 174 (2016) 209.
13. J. H. Li, Q. Liu, Y. L. Wang, R. R. Chen, K. Takahashi, R. M. Li, L. H. Liu, J. Wang, *J. Electrochem. Soc.*, 163 (2016) 62.
14. J. L. Song, Y. Lu, S. Huang, X. Liu, L. B. Wu, W. J. Xu, *Appl. Surf. Sci.*, 266 (2013) 445.
15. Q. Liu, D. X. Chen, Z. X. Kang, *ACS Appl. Mater. Inter.*, 7 (2015) 1859.
16. Z. Q. Qian, S.D. Wang, X.S. Ye, Z. Liu, Z. J. Wu, *Appl. Surf. Sci.*, 453 (2018) 1.
17. H. Liu, J.Y. Huang, Z. Chen, G.Q. Chen, K.Q. Zhang, S. Salem, Al Deyab, Y.K. Lai, *Chem. Eng. J.*, 330 (2017) 26.
18. Z.H. Wang, L. Yuan, G. Z. Liang, A. J. Gu, *Chem. Eng. J.*, 408 (2021) 127263.
19. J. Gao, L. Wu, G. Zheng, J. Li, X. Cong, H. Xue, *J Mater. Chem. C.*, 14 (2019) 4199.
20. P. Wang, T. Zhao, R. Bian, G. Wang, H. Liu, *ACS Nano*, 11 (2017) 12385.
21. L.Y. Meng, S. J. Park. *Carbon*, 2 (2014) 89.
22. Y. P. Zhang, H. Z. Zhu, C. Zhuang, S. G. Chen, L. Q. Wang, L. H. Dong, Y. S. Yin, *Mater. Chem. Phys.*, 179 (2016) 80.
23. X. Ouyang, X. Qiu, H. M. Lou, D. J. Yang, *Ind. Eng. Chem. Res.*, 45 (2006) 5716.
24. Y. Liu, H. Cao, Y. Yu, S. G. Chen, *Int. J. Electrochem. Sc.*, 10 (2015) 3497.
25. H. Ogihara, J. Xie, T. Saji, *J. Mater. Sci.*, 49 (2014) 3183.
26. E. Celia, T. Darmanin, E. R. de Givenchy, S. Amigoni, F. Guittard, *J. Colloid. Inter. Sci.*, 402 (2013) 1.

27. Z. J. Wu, I. S. Ahn, C. H. Lee, J. H. Kim, Y. G. Shul, S. K. Lee, *Colloids Surf. A*, 240 (2004) 157.
28. I. Jerman, B. Orel, A. Š. Vuk, M. Koželj, J. Kovač, *Thin Solid Films*, 518 (2010,) 2710.
29. Y. Zhang, H. Zhu, C. Zhuang, S. G. Chen, L. Q. Wang, L. H. Dong, Y. S. Yin, *Mater. Chem. Physics.*, 179 (2016) 80.
30. A. Vilčnik, I. Jerman, A. Š. Vuk, M. Koželj, B. Orel, *Langmuir*, 25 (2009), 5869.
31. J. Shen, Y. Hu, C. Li, C. Qin, M. Ye, *Electrochim. Acta*, 53 (2008) 7276.
32. Q. Ta, Z. Gao, J. Yan, D. Xia, W. Hu. *Prog. Org. Coat.*, 146 (2020) 105675.
33. F. Su, K. Yao. *ACS Appl. Mater. Inter.*, 6 (2014) 8762.
34. Y. Zhou, Y. Ma, Y. Sun, Z. Xiong, C. Qi, Y. Zhang, Y. Liu. *ACS Appl. Mater. Inter.*, 11 (2019) 6512.
35. Y. Liu, H. Cao, Y. Yu, S. G. Chen, *Int. J. Electrochem. Sc.*, 10 (2015) 3497.
36. S. Chen, Y. Cai, Z. Chen, M. Y. Yu, X. W. Song, Y. P. Zhang, *Appl. Surf. Sci.*, 331 (2015) 315.
37. J. Cai, S. Wang, J. H. Zhang, Y. Liu, T. Hang, H. Q. Ling, M. Li, *Appl. Surf. Sci.*, 436 (2018) 950.
38. Y. Liu, X. Yin, J. Zhang, S. Y, Z. Han, L. Ren. *Electrochim. Acta*, 125 (2014) 395.
39. Y. Liu, W. Yao, X. Yin, H. Wang, Z. Han, L. Ren, *Adv. Mater. Interfaces*, 3 (2016), 1500723.
40. S. Zhou, X. Zhu, Q. Yan, *Surf. Interf. Anal.*, 50 (2017) 290.
41. Y. Cheng, S. Lu, W. Xu, K. B. Cao, J. Y. Li, Y. Zheng, *Surf. Coat. Tech.*, 333 (2017) 61.

© 2022 The Authors. Published by ESG (www.electrochemsci.org). This article is an open access article distributed under the terms and conditions of the Creative Commons Attribution license (<http://creativecommons.org/licenses/by/4.0/>).